Correlating Structure, Conductance, and Mechanics of Silver Atomic-Scale Contacts

Sriharsha V. Aradhya,[†,§] Michael Frei,[†,§] András Halbritter,[‡] and Latha Venkataraman[†,*]

[†]Department of Applied Physics and Applied Mathematics, Columbia University, New York, NY, United States, and [‡]Department of Physics, Budapest University of Technology and Economics and Condensed Matter Research Group of the Hungarian Academy of Sciences, Hungary. [§]S.V.A. and M.F. contributed equally to this study.

ABSTRACT We measure simultaneously force and conductance of Ag metal point-contacts under ambient conditions at room temperature. We observe the formation of contacts with a conductance close to 1 G_0, the quantum of conductance, which can be attributed to a single-atom contact, similar to those formed by Au. We also find two additional conductance features at ~0.4 G_0 and ~1.3 G_0, which have been previously ascribed to contacts with oxygen contaminations. Here, using a conductance cross-correlation technique, we distinguish three different atomic-scale structural motifs and analyze their rupture forces and stiffness. Our results allow us to assign the ~0.4 G_0 conductance feature to an Ag—O—Ag contact and the ~1.3 G_0 feature to an Ag—Ag single-atom contact with an oxygen atom in parallel. Utilizing complementary information from force and conductance, we thus demonstrate the correlation of conductance with the structural evolution at the atomic scale.

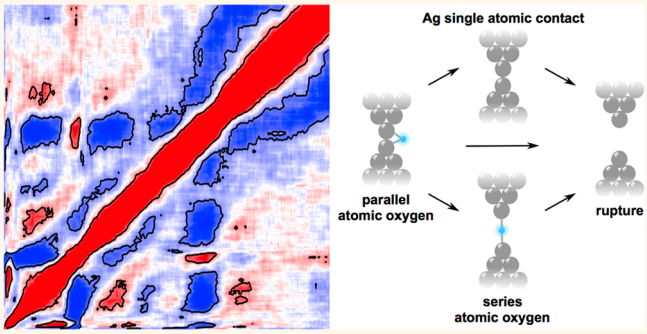

KEYWORDS: bond rupture forces · Ag point-contacts · atomic defects · electronic transport · break-junctions

The electronic properties of metal single-atom contacts have been studied extensively using the mechanically controlled break-junction technique and the scanning tunneling microscope based break-junction technique.[1] The most commonly studied metal in such measurements is gold (Au) due to its chemical stability in ambient conditions, and its relative ease in metallizing various surfaces. Electronic measurements with a series of other metals have been carried out under ultrahigh or high-vacuum conditions;[2−8] however, there are very few studies of the mechanical properties of these nanoscale wires and point-contacts for metals other than Au.[9] In this paper, we present simultaneous force and conductance measurements of silver (Ag) atomic contacts and compare their properties with Au contacts. Whereas Au atomic contacts show a clear 1 G_0 ($G_0 = 2e^2/h$, the quantum of conductance) feature corresponding to the formation of single atomic contacts even under ambient conditions, Ag shows additional features at ~0.4 G_0 and ~1.3 G_0. Such conductance features have been observed in previous experimental studies,[10−12] and theoretical investigations[13−16] have provided detailed insight into their structural origin. In particular, molecular O_2 is known to dissociate into atomic O and adsorb to undercoordinated Ag atoms, even at temperatures as low as 105 K.[17−19] An oxygen atom can therefore be expected to bond to the highly reactive Ag atomic-size contact, and bridge an Ag—Ag contact either in parallel or in series as Ag—O—Ag. Such events are more pronounced in Ag compared to Au, due to its higher reactivity.[11,20] Measurements with Ag point contacts therefore present richer possibilities in structure and evolution under elongation when compared with Au single atomic contacts and also open up the possibility to study *in situ* reactions that could lead to the formation of novel single-molecule junctions.[21]

In this study, we measure, simultaneously, the electronic and mechanical properties of Ag point contacts using a custom atomic force microscope to probe the formation

* Address correspondence to lv2117@columbia.edu.

Received for review February 11, 2013 and accepted March 22, 2013.

Published online March 23, 2013
10.1021/nn4007187

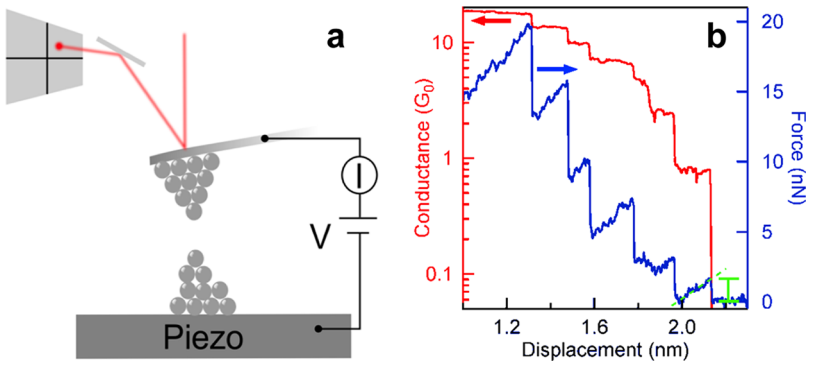

Figure 1. (a) Schematic of the experimental setup used for simultaneous force and conductance measurements. (b) Sample trace showing the evolution of conductance (red, left axis) and force (blue, right axis) for a Ag point contact as a function of junction elongation. The drop in force at the end of the conductance step corresponds to the rupture force, while the slope of the force trace over the conductance plateau is related to the stiffness of the junction.

and evolution of Ag contacts under ambient conditions. We measure thousands of junctions to carry out a statistical analysis in a robust manner. We find that during the thinning of Ag point contacts under junction elongation, there are not only conductance plateaus due to Ag single-atom contacts (with conductance of ~1 G_0), but also plateaus at ~0.4 G_0 and ~1.3 G_0 which we assign to the presence of atomic oxygen impurities. Although we cannot rule out the presence of other impurities in our experiments, our observed experimental evidence is consistent with previous experimental[10−12] and theoretical[13−16] studies, which attribute these conductance features to atomic oxygen in Ag contacts. We use a cross-correlation technique[22,23] to study the mutual conditional occurrence of these three conductance features in a statistically robust manner. The insights from these cross-correlations allow us to employ a simple algorithm to sort junctions based on their structures into three distinct groups: (a) junctions with a single Ag-atom contact (Ag-SAC); (b) a single Ag-atom contact with a parallel oxygen atom bridge (AgO-P) and (c) a single-Ag-atom contact incorporating an oxygen atom in series (AgO-S). We deduce the structural evolution pathways for these junctions and analyze the force data to quantify the mechanics of the three distinct contacts. We find that the 1 G_0 conductance features, which arise from Ag single atomic contacts, have a rupture force of 1 nN and a stiffness of 8 N/m. The 0.4 G_0 features, which are attributed to the configuration with an oxygen atom in series, have slightly lower rupture forces (0.8 nN) but have a stiffness (8 N/m) comparable to that of the single Ag-atom contact. In contrast, structures with oxygen in parallel (with a conductance of ~1.3 G_0) show a significantly higher rupture force (1.7 nN) and a higher stiffness (14 N/m). Together, these quantitative results not only represent the first direct measurement of the mechanics of Ag point-contacts, but also allow us to unambiguously conclude that the Ag−O bonds are comparable in strength to the Ag−Ag bonds and mechanically stabilize Ag contacts when O atoms are in a parallel configuration.

RESULTS AND DISCUSSION

We carry out simultaneous conductance and force measurements using an atomic force microscope based break-junction method (AFM-BJ). To gather larger statistics on conductance correlations, we also carry out conductance measurements alone in a scanning tunneling microscope based break-junction setup (STM-BJ).[24] The AFM experimental setup and analytical procedures are detailed in the Methods section, and have also been described in detail previously.[25,26] Briefly, a Ag-coated AFM cantilever and a freshly mechanically polished Ag substrate are repeatedly brought in and out of contact using a high resolution piezo positioner at a constant velocity. Conductance is measured across the tip/sample junction at constant bias of 25 mV. The force is measured simultaneously by monitoring the deflection of a laser focused on the back of the cantilever as schematically illustrated in Figure 1a. Figure 1b shows conductance (red) and force (blue) measurements from a typical Ag junction elongation and rupture. Conductance decreases stepwise as a function of displacement, similar to what is observed for Au point-contacts.[1] The simultaneously measured force traces show a typical sawtooth pattern attributed to reversible (elastic) and irreversible (plastic) deformations.[27]

Characteristic Conductance Features. To understand the details of the different conductance plateaus seen with these traces, we first collect a large data set of 10 000 Ag conductance traces with the STM-BJ setup as it is easier to gather large data sets with a Ag wire tip in the STM as opposed to using a Ag-coated cantilever necessary for the AFM-BJ measurements. We analyze the conductance traces by creating a linear-binned histogram without data selection. Figure 2a compares 1D conductance histograms (normalized by the number of included traces) for Ag (gray) with that for Au (yellow). Both histograms reveal characteristic peaks at well-defined conductance values, although the peaks

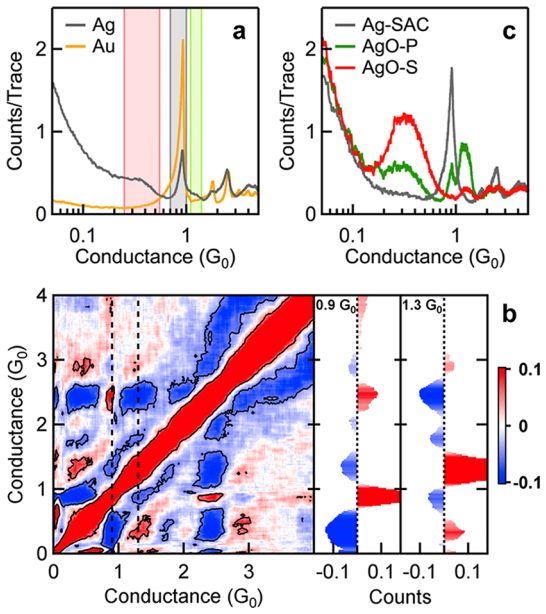

Figure 2. (a) One-dimensional conductance histograms (linearly binned, bin size 0.001 G_0) constructed without any data selection for 10 000 Ag (gray) traces; Au (gold) histogram is shown for comparison. These traces were measured with the STM-BJ setup. The highlighted regions indicate conductance ranges associated with AgO-S (red), Ag-SAC (gray), and AgO-P (green). (b) 2D cross-correlation histogram constructed without data selection for Ag traces. The panels on the right are profiles along the dotted lines shown on the cross-correlation histogram, at 0.9 G_0 and 1.3 G_0, respectively. The scale bar indicates the color scale used for the correlation values: red, positive; blue, negative; and white, zero correlation. The black contours are at ±0.05. (c) One-dimensional conductance histograms constructed from selected traces that have at least 80 data points in the Ag-SAC (gray, 3904 traces), AgO-S (red, 3345 traces), and AgO-P (green, 2501 traces) conductance ranges, respectively.

are more prominent for the Au measurements. As in Au, a 1 G_0 conductance plateau in Ag corresponds to a junction with a single conducting channel with unit transmission.[8,28−31] However, it is known that Ag contacts do not form long single atomic chains;[8,28−31] indeed, we see a reduced 1 G_0 peak as Ag plateaus are considerably shorter. Additionally, the Ag histogram peak does not show a clear peak around 1.8 G_0, unlike the Au histogram, but a peak around 2.5 G_0 is clearly visible. This higher conductance peak at ∼2.5 G_0 has been attributed to a stable contact geometry with a triangular (3-atom) cross-section.[8,31] The Ag measurements also show a large number of counts below 1 G_0, corresponding to larger through-space tunneling currents after junction rupture, indicating that the dynamics of the atomic-scale relaxation of Ag single-atom contacts immediately after rupture is different from Au contacts.[12,30,32] The presence of other adsorbates around the junction could also be responsible for the counts at lower conductance values in Ag junctions.

The Ag histogram in Figure 2a also shows a feature around 0.4 G_0 indicating that a frequent and stable configuration with that conductance is formed when Ag contacts are broken.[10−12] Since O_2 from the ambient environment can dissociate on under-coordinated silver atoms,[17−19] we can expect oxygen atoms to interact with the Ag point-contacts to form Ag−O containing structures. Theoretically, Ag-single atom contacts with an O in series were shown to have a conductance of ∼0.4 G_0.[13,16] Furthermore, it was shown experimentally that the 1 G_0 single atom contact feature in 1D conductance histograms was suppressed when traces showing 1.3 G_0 and 0.4 G_0 features were selectively analyzed.[10] These results highlight the need to better understand the structure and structural evolution basis for the observations. In what follows, we utilize the independently measured conductance and force data to determine the structural evolution pathway by first quantifying the correlations in the occurrence of different structures using conductance as their structural fingerprint and then analyzing the mechanical properties of each of these structures.

Correlations among Conductance Features. We first carry out a statistical correlation analysis for the measured conductance traces by constructing a two-dimensional cross-correlation histogram (Figure 2b), using a procedure detailed previously[22,23] (see Supporting Information). Briefly, the 2D cross-correlation histogram shows the correlation in either the occurrence or in the plateau lengths of different conductance features within individual traces. Positively (negatively) correlated regions indicate that two conductance values occur (do not occur) together in the same trace frequently.[22] In Figure 2b (right panel), we also plot a vertical profile of this 2D correlation plot taken at ∼1 G_0 (corresponding to the dashed line at 0.9 G_0 on the cross-correlation histogram) where correlations between a 1 G_0 feature and those at other conductance values are elucidated. Along this line profile, the red, positively correlated region around 2.5 G_0 indicates that plateaus around 1 G_0 and 2.5 G_0 frequently occur together in the same trace. In contrast, the blue regions around 0.4 G_0 and 1.3 G_0, which we attributed to the presence of O in the junction, indicate that 1 G_0 plateaus are anticorrelated with plateaus at either of these values. Next, we consider a vertical section around 1.3 G_0 (corresponding to the dashed line at 1.3 G_0 on the cross-correlation histogram, Figure 2b). Along this profile, the red regions around 0.4 G_0 indicate that the structures responsible for conductance plateaus at 1.3 G_0 and 0.4 G_0 are correlated.

A subtle, but important detail in the analysis of cross-correlation histograms is that the negative values in the cross-correlation histogram can stem from two reasons: (a) anticorrelations in occurrence (occurrence of two conductance plateaus is mutually exclusive), or (b) anticorrelations in plateau lengths (longer plateau length at one conductance value is accompanied by a shorter plateau length at the other conductance, and

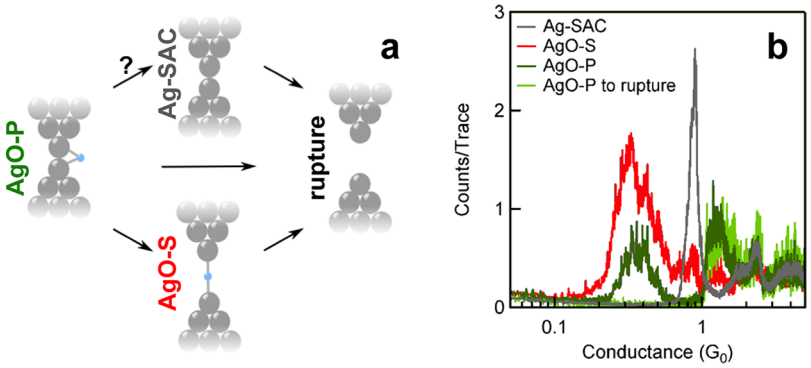

Figure 3. (a) Schematic illustration of the three bonding motifs representing a clean Ag single atomic contact (Ag-SAC), Ag atomic contact with a series O bridge (AgO-S), Ag atomic contact with a parallel O bridge (AgO-P), and a ruptured junction. Arrows indicate the experimentally inferred structural evolution pathways. (b) One-dimensional conductance histograms constructed from selected AFM-BJ traces for Ag-SAC (gray, 955 traces), AgO-S (red, 355 traces), AgO-P (dark green, 214 traces), and AgO-P to rupture (light green, 90 traces).

vice versa). To determine whether the anticorrelation between the 1 G_0 plateau and those at 1.3 G_0 and 0.4 G_0 is due to the an anticorrelation in their occurrence or anticorrelation in their plateau lengths, we construct conditional histograms[22,23] from subsets of all measured traces, selecting for conductance features defined by the highlighted regions in Figure 2a. Specifically, we first select traces that have more than 80 data points (equivalent to a minimum plateau length of ~0.015 nm) within one of the three conductance ranges: 0.7−1.0 G_0 for Ag-SAC region, 0.25−0.55 G_0 for the AgO-S region, and 1.1−1.4 G_0 for the AgO-P region. These conductance ranges and the plateau length cutoff are determined from a logarithmically binned conductance histogram as detailed in the Methods section. We then construct conditional 1D histograms (Figure 2c) of the selected traces, without any other selection criteria. We observe that by selecting for the Ag-SAC plateaus, both the AgO-S and AgO-P features are highly suppressed, whereas the 2.5 G_0 feature is retained. This indicates that clean Ag-SAC junctions occur when oxygen impurities are absent in the vicinity of the junction. This result is in agreement with the cross-correlation analysis in Figure 2a, and with data from Ag contacts measured in an oxygen-free high-vacuum environment.[8] Similarly, by selecting for AgO-S conductance there is a dramatic suppression of the Ag-SAC feature. This supports the finding from the cross-correlation analysis that AgO-S and Ag-SAC junctions do not occur in the same trace. On the other hand, by selecting for the AgO-P conductance we note that the Ag-SAC feature is reduced, but not fully suppressed. This could imply that occasionally Ag-SACs occur after the AgO-P junction, with anticorrelated plateau lengths.[22] However, since the AgO-P and Ag-SAC conductance ranges are close, it is also possible that when we select traces with AgO-P features, we inadvertently pick a trace with Ag-SAC plateau. This is because the tail of the 1 G_0 histogram peak extends above 1 G_0, as is most clearly visible for the Au data (Figure 2a).

These structural insights are summarized as a schematic illustration in Figure 3a, which shows the structural transition pathways for the Ag and Ag/O junctions. This scheme motivates the use of conductance features combined with simultaneous force measurements to quantify the mechanics of the various structural evolution scenarios of these atomic-scale junctions. Whereas AgO-S and Ag-SAC junctions rupture upon elongation, AgO-P junctions can rupture to an open contact, or evolve into an AgO-S or, perhaps, into an Ag-SAC junction. In our analysis of forces, we treat these categories separately.

Mechanics of Distinct Structural Motifs. We now analyze the data acquired using the AFM-BJ setup where we measure force simultaneously with conductance in 6 500 junctions. We first sort all measured traces to differentiate the structures based on the conductance features as detailed above. We further ensure that the Ag-SAC and AgO-S junctions rupture under elongation by selecting those traces where the conductance after rupture goes below 0.01 G_0 within 80 data points. For the AgO-P junctions, we only include traces which have less than 80 data points in the Ag-SAC conductance range (0.7−1.0 G_0) and fewer than 80 data points in the 0.01−0.25 G_0 conductance range as detailed above. With these requirements, we only include AgO-P junctions that evolve to AgO-S junctions or that rupture completely (Figure 3a). To characterize the subset of AgO-P junctions which rupture without evolving into an AgO-S structure, we select AgO-P junctions that have less than 80 data points in the 0.01−1.0 G_0 conductance range, thereby excluding Ag-SAC and AgO-S conductance features that could occur after the AgO-P conductance plateau. We note that not every conductance trace among the data set (consisting of 6 500 simultaneous measurements of conductance and force) contains one of these structures of interest. Normalized conductance histograms from these selected subsets are shown in Figure 3b, which has the same peaks as those shown in Figure 2b, but

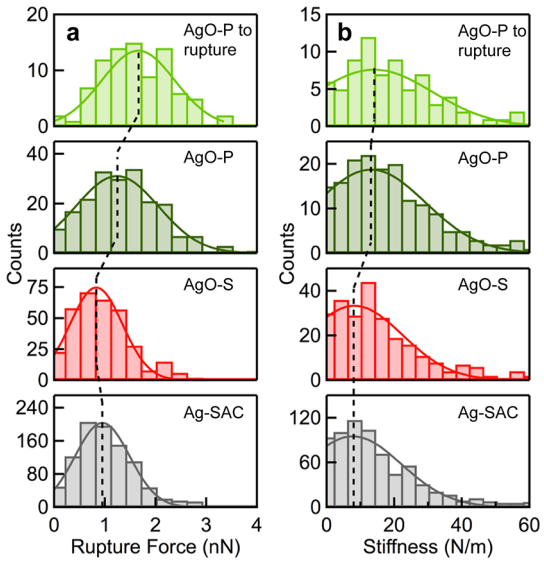

Figure 4. (a) Histograms of rupture force and (b) stiffness for Ag-SAC (gray), AgO-S (red), AgO-P (dark green), and AgO-P to rupture (light green). Gaussian fits are overlaid as solid curves and the dashed lines are provided as visual guides connecting the peak values.

very few counts in the low-conductance region, as traces that contribute to this region have been excluded in the selection. Peaks at 1 G_0 and 0.4 G_0 are seen in the Ag-SAC and AgO-S scenarios, analogous to those in Figure 2b. For the AgO-P junctions that rupture completely, a peak at 1.3 G_0 is observed. For the selection that includes AgO-P junctions that evolve into an AgO-S junction, we see an additional conductance peak in the AgO-S range.

We can now analyze the simultaneously measured force data to determine rupture force and stiffness of individual junctions, for each of the four types of traces selected above (see Supporting Information for sample traces). We begin by locating the displacement range corresponding to the conductance plateau of interest (Figure 3b). We then obtain the rupture force by determining the force drop at the position where the conductance plateau ends, that is, where the conductance drops abruptly below the plateau level (as illustrated in Figure 1b). We determine the stiffness of the junction by extracting the slope of the force ramp prior to the sharp drop (dotted line, Figure 1b). Since the force trace shows additional features during the course of a conductance plateau due to atomic-scale rearrangement, we use an automated algorithm[26] to isolate the final force event and use the slope of this segment to reliably obtain the stiffness of the junction (see Supporting Information). This measured stiffness is the stiffness of the entire junction and also includes the stiffness of the cantilever. To determine the junction stiffness, we correct the measured value using a series spring model for the measured spring constant[33] of the AFM cantilever (~50 N/m) for each junction. Histograms of rupture force and stiffness are shown in

TABLE 1. Most Frequently Measured Force and Stiffness. Sample Size for Each Case and Standard Errors in the Fit Are Also Shown

type	no. of traces	force (nN)	stiffness (N/m)
Ag-SAC	955	0.95 ± 0.02	7.7 ± 0.5
AgO-S	344	0.83 ± 0.03	8.2 ± 0.8
AgO-P	215	1.24 ± 0.06	13.1 ± 1.2
AgO-P to rupture	90	1.66 ± 0.09	14.1 ± 2.1

Figure 4a,b along with Gaussian fits used to determine the mean rupture force and stiffness for each junction type. The results are from this analysis are summarized in Table 1.

We first observe that the measured rupture force for Ag-SACs (1 nN) is significantly smaller than that of an Au single-atom contact (1.5 nN).[25−27] This is in excellent agreement with previous theoretical calculations that have consistently found a lower rupture force of ~1 nN for Ag-SACs compared to ~1.5 nN for Au.[14,34−37] The stiffness of Ag-SACs of 8 N/m is the same as that measured for Au,[26,27] perhaps reflecting the similar bulk Young's modulus of Ag and Au (~80 GPa).[38]

The AgO-S junctions have a slightly smaller rupture force (0.8 nN) than Ag-SAC junctions, and stiffness (8 N/m) equal to the Ag-SAC junctions, within experimental error. When the interatomic bonds are represented as springs in a simplified model, in a AgO-S junction, the two Ag−O bonds are in series with the Ag electrodes, and thus its stiffness and rupture force can only be smaller than or equal to that of an Ag-SAC (Figure 3a). Theoretical calculations indicate that the Ag−O bond strength might be comparable to the Ag−Ag bond in the Ag-SAC case.[14,34] Experimentally, the observation of enhanced formation of monatomic Ag wires in low-temperature break-junction experiments (<40 K) in the presence of oxygen also supports the idea that Ag−O bonds are comparable in strength to Ag−Ag bonds.[11,12] Our experimental results thus present a quantitative measurement of the Ag−O bonding strength.

For the AgO-P junctions that rupture completely, we obtain a rupture force (stiffness) of 1.7 nN (14 N/m) when the junction ruptures to an open contact. However, if the AgO-P junctions that evolve to AgO-S junctions are included, the rupture force and stiffness are found to be 1.2 nN and 13 N/m respectively. The rupture force for an AgO-P junction is thus much larger than for Ag-SAC and AgO-S. This strongly indicates that the oxygen atom is stabilizing the junction in AgO-P junctions. In an AgO-P configuration (Figure 3a) we expect the Ag−O bonds to be in parallel to the Ag−Ag bonds; such a junction will be stiffer than Ag-SAC, and if it ruptures upon elongation, we expect a larger rupture force than that of an Ag-SAC. The stiffness and rupture force results obtained here provide conclusive evidence that the 1.3 G_0 junctions are indeed those that have an O in a parallel configuration. The fact that the

stiffness of AgO-S junctions is almost the same as Ag-SAC junctions further demonstrates that the Ag−O bonds are comparable to Ag−Ag bonds in terms of their mechanical properties. On the other hand, the parallel Ag−O bonds in AgO-P junctions can be intuitively thought of as providing additional stabilization, as well as a parallel spring in the junction. Finally, we note a subtlety in interpreting the meaning of the measured rupture force of AgO-P junctions. The lower rupture force in AgO-P junctions which evolve into a AgO-S structure is due to the fact that the junction does not rupture to an open contact. This prevents the AFM cantilever from relaxing completely and therefore the measured drop in force is smaller than the full value that is observed in the AgO-P junctions that rupture to a conductance below the 0.01 G_0 cutoff. Therefore, in this context, the measured forces correspond to the difference between the maximum sustained force by AgO-P junctions and the initial force sustained by the succeeding AgO-S junction. However, the measured stiffness is approximately the same (within experimental error) for AgO-P junctions, whether considering only the subset of junctions that ruptures or including junctions that evolve into AgO-S structures as well, since the basic AgO-P structure is the same, irrespective of the evolution scenarios.

CONCLUSIONS

We have studied the electric and mechanical behavior of Ag junctions in ambient conditions. These measurements show conductance features of clean Ag-SACs as well as Ag contacts that include O impurities. Using a selection process based on the cross-correlations among the conductance of various junction structures, we are able to analyze different junction structures separately. The results from the force measurements allow us to rigorously quantify the mechanics of Ag-SAC, AgO-S, and AgO-P structures, adding significantly to our understanding of the behavior of atomic-size junctions of Ag, and their contrast with Au. We expect the experimental methods and results presented here to enable progress in the study of single molecule junctions with Ag electrodes.

METHODS

Experimental Setup. Conducting AFM measurements are carried out using a custom built setup which consists of a modified commercial AFM head (Veeco Multimode) which has been optimized for high signal-to-noise ratio with custom optics and electronic components. We use commercial filters, adders (SRS), data acquisition systems (National Instruments PXI), and current amplifier (Keithley 428) for the conductance and force measurements. We use a high-resolution 24-bit PXI-4461 card to move a calibrated single-axis piezoelectric positioner (MadCity Labs) at a constant speed of 18 nm/s during junction elongation. The Ag-coated AFM cantilevers were prepared by evaporating ~300 nm of Ag using a thermal evaporator (Edwards BOC/Auto 306). The AFM cantilevers have a stiffness of ~50 N/m, and were calibrated by measuring their thermal spectrum. Freshly mechanically polished Ag disks (Alfa Aesar) were used as substrates. Measurements were performed soon after the metal deposition/polishing, without any additional chemical treatment to the deposited surfaces. At the beginning of each trace, we ensure that the conductance is larger than 5 G_0 ($G_0 = 2e^2/h$, "quantum of conductance") in order to sample a wide variety of junctions during the measurements.

Data Analysis. We construct logarithmically binned 1D histograms for the conductance traces (see Supporting Information, Figure S1). This histogram allows us to locate the peaks and minima in the conductance histogram and assign the conductance ranges for Ag-SAC, AgO-S, and AgO-P junctions. We sum the counts in the histogram under each of these conductance ranges: the Ag-SAC feature on average has 120 data points, the AgO-S feature has 125 data points, and the AgO-P feature has 80 data points per trace. Therefore we select traces which have at least 80 data points in a particular conductance range to ensure the existence of a structure corresponding to that conductance range.

Conflict of Interest: The authors declare no competing financial interest.

Acknowledgment. This work was supported by NSF Career Award CHE-07-44185 and by the Packard Foundation. A.H. acknowledges support from the OTKA K105735 research grant.

Supporting Information Available: Additional experimental data, analysis details and a description of the cross-correlation analysis. This material is available free of charge *via* the Internet at http://pubs.acs.org.

REFERENCES AND NOTES

1. Agraït, N.; Yeyati, A. L.; van Ruitenbeek, J. M. Quantum Properties of Atomic-Sized Conductors. *Phys. Rep.* **2003**, *377*, 81–279.
2. Krans, J. M.; Muller, C. J.; Yanson, I. K.; Govaert, T. C. M.; Hesper, R.; van Ruitenbeek, J. M. One-Atom Point Contacts. *Phys. Rev. B* **1993**, *48*, 14721–14724.
3. Krans, J. M.; van Ruitenbeek, J. M.; Fisun, V. V.; Yanson, I. K.; Dejongh, L. J. The Signature of Conductance Quantization in Metallic Point Contacts. *Nature* **1995**, *375*, 767–769.
4. Scheer, E.; Agrait, N.; Cuevas, J. C.; Yeyati, A. L.; Ludoph, B.; Martin-Rodero, A.; Bollinger, G. R.; van Ruitenbeek, J. M.; Urbina, C. The Signature of Chemical Valence in the Electrical Conduction through a Single-Atom Contact. *Nature* **1998**, *394*, 154–157.
5. Oshima, H.; Miyano, K. Spin-Dependent Conductance Quantization in Nickel Point Contacts. *Appl. Phys. Lett.* **1998**, *73*, 2203–2205.
6. Ludoph, B.; van der Post, N.; Bratus', E. N.; Bezuglyi, E. V.; Shumeiko, V. S.; Wendin, G.; van Ruitenbeek, J. M. Multiple Andreev Reflection in Single-Atom Niobium Junctions. *Phys. Rev. B* **2000**, *61*, 8561–8569.
7. Costa-Kramer, J. L. Conductance Quantization at Room Temperature in Magnetic and Nonmagnetic Metallic Nanowires. *Phys. Rev. B* **1997**, *55*, R4875–R4878.
8. Rodrigues, V.; Bettini, J.; Rocha, A. R.; Rego, L. G. C.; Ugarte, D. Quantum Conductance in Silver Nanowires: Correlation between Atomic Structure and Transport Properties. *Phys. Rev. B* **2002**, *65*, 153402.
9. Masuda, H.; Kizuka, T. Structure, Electrical, and Mechanical Properties of Silver Nanocontacts. *Jpn. J. Appl. Phys.* **2010**, *49*, 045202.
10. den Boer, D.; Shklyarevskii, O. I.; Coenen, M. J. J.; van der Maas, M.; Peters, T. P. J.; Elemans, J. A. A. W. Speller, S. Mechano-Catalysis: Cyclohexane Oxidation in a Silver Nanowire Break Junction. *J. Phys. Chem. C* **2011**, *115*, 8295–8299.
11. Thijssen, W. H. A.; Marjenburgh, D.; Bremmer, R. H.; van Ruitenbeek, J. M. Oxygen-Enhanced Atomic Chain Formation. *Phys. Rev. Lett.* **2006**, *96*, 026806.

12. Thijssen, W. H. A.; Strange, M.; de Brugh, J. M. J. A.; van Ruitenbeek, J. M. Formation and Properties of Metal-Oxygen Atomic Chains. *New J. Phys.* **2008**, *10*, 033005.
13. Ishida, H. Embedded Green-Function Calculation of the Conductance of Oxygen-Incorporated Au and Ag Monatomic Wires. *Phys. Rev. B* **2007**, *75*, 205419.
14. Di Napoli, S.; Thiess, A.; Blugel, S.; Mokrousov, Y. Modeling Impurity-Assisted Chain Creation in Noble-Metal Break Junctions. *J. Phys. Condens. Mater.* **2012**, *24*, 135501.
15. Thiess, A.; Mokrousov, Y.; Blugel, S.; Heinze, S. Theory and Application of Chain Formation in Break Junctions. *Nano Lett.* **2008**, *8*, 2144–2149.
16. Strange, M.; Thygesen, K. S.; Sethna, J. P.; Jacobsen, K. W. Anomalous Conductance Oscillations and Half-Metallicity in Atomic Ag-O Chains. *Phys. Rev. Lett.* **2008**, *101*, 096804.
17. Bonini, N.; Kokalj, A.; Dal Corso, A.; de Gironcoli, S.; Baroni, S. Structure and Dynamics of Oxygen Adsorbed on Ag(100) Vicinal Surfaces. *Phys. Rev. B* **2004**, *69*, 195401.
18. Vattuone, L.; Burghaus, U.; Savio, L.; Rocca, M.; Costantini, G.; de Mongeot, F. B.; Boragno, C.; Rusponi, S.; Valbusa, U. Oxygen Interaction with Disordered and Nanostructured Ag(001) Surfaces. *J. Chem. Phys.* **2001**, *115*, 3346–3355.
19. Schmidt, M.; Cahuzac, P.; Brechignac, C.; Cheng, H. P. The Stability of Free and Oxidized Silver Clusters. *J. Chem. Phys.* **2003**, *118*, 10956–10962.
20. Jelinek, P.; Perez, R.; Ortega, J.; Flores, F. *Ab Initio* Study of Evolution of Mechanical and Transport Properties of Clean and Contaminated Au Nanowires Along the Deformation Path. *Phys. Rev. B* **2008**, *77*, 115447.
21. Cheng, Z. L.; Skouta, R.; Vázquez, H.; Widawsky, J. R.; Schneebeli, S.; Chen, W.; Hybertsen, M. S.; Breslow, R.; Venkataraman, L. *In Situ* Formation of Highly Conducting Covalent Au-C Contacts for Single-Molecule Junctions. *Nat. Nanotechnol.* **2011**, *6*, 353–357.
22. Makk, P.; Tomaszewski, D.; Martinek, J.; Balogh, Z.; Csonka, S.; Wawrzyniak, M.; Frei, M.; Venkataraman, L.; Halbritter, A. Correlation Analysis of Atomic and Single-Molecule Junction Conductance. *ACS Nano* **2012**, *6*, 3411–3423.
23. Halbritter, A.; Makk, P.; Mackowiak, S.; Csonka, S.; Wawrzyniak, M.; Martinek, J. Regular Atomic Narrowing of Ni, Fe, and V Nanowires Resolved by Two-Dimensional Correlation Analysis. *Phys. Rev. Lett.* **2010**, *105*, 266805.
24. Venkataraman, L.; Klare, J. E.; Tam, I. W.; Nuckolls, C.; Hybertsen, M. S.; Steigerwald, M. L. Single-Molecule Circuits with Well-Defined Molecular Conductance. *Nano Lett.* **2006**, *6*, 458–462.
25. Frei, M.; Aradhya, S. V.; Koentopp, M.; Hybertsen, M. S.; Venkataraman, L. Mechanics and Chemistry: Single Molecule Bond Rupture Forces Correlate with Molecular Backbone Structure. *Nano Lett.* **2011**, *11*, 1518–1523.
26. Aradhya, S. V.; Frei, M.; Hybertsen, M. S.; Venkataraman, L. Van Der Waals Interactions at Metal/Organic Interfaces at the Single-Molecule Level. *Nat. Mater.* **2012**, *11*, 872–876.
27. Rubio-Bollinger, G.; Bahn, S.; Agraït, N.; Jacobsen, K.; Vieira, S. Mechanical Properties and Formation Mechanisms of a Wire of Single Gold Atoms. *Phys. Rev. Lett.* **2001**, *87*, 026101.
28. Smit, R. H. M.; Untiedt, C.; Yanson, A. I.; van Ruitenbeek, J. M. Common Origin for Surface Reconstruction and the Formation of Chains of Metal Atoms. *Phys. Rev. Lett.* **2001**, *87*, 266102.
29. Ludoph, B.; van Ruitenbeek, J. M. Conductance Fluctuations as a Tool for Investigating the Quantum Modes in Atomic-Size Metallic Contacts. *Phys. Rev. B* **2000**, *61*, 2273–2285.
30. Kaneko, S.; Nakazumi, T.; Kiguchi, M. Fabrication of a Well-Defined Single Benzene Molecule Junction Using Ag Electrodes. *J. Phys. Chem. Lett.* **2010**, *1*, 3520–3523.
31. Hansen, K.; Laegsgaard, E.; Stensgaard, I.; Besenbacher, F. Quantized Conductance in Relays. *Phys. Rev. B* **1997**, *56*, 2208–2220.
32. Yanson, A. I.; Bollinger, G. R.; van den Brom, H. E.; Agrait, N.; van Ruitenbeek, J. M. Formation and Manipulation of a Metallic Wire of Single Gold Atoms. *Nature* **1998**, *395*, 783–785.
33. Hutter, J. L.; Bechhoefer, J. Calibration of Atomic-Force Microscope Tips. *Rev. Sci. Instrum.* **1993**, *64*, 1868–1873.
34. Cakir, D.; Gulseren, O. Effect of Impurities on the Mechanical and Electronic Properties of Au, Ag, and Cu Monatomic Chain Nanowires. *Phys. Rev. B* **2011**, *84*, 085450.
35. Bahn, S. R.; Jacobsen, K. W. Chain Formation of Metal Atoms. *Phys. Rev. Lett.* **2001**, *87*, 266101.
36. Ribeiro, F. J.; Cohen, M. L. *Ab Initio* Pseudopotential Calculations of Infinite Monatomic Chains of Au, Al, Ag, Pd, Rh, and Ru. *Phys. Rev. B* **2003**, *68*, 035423.
37. Zarechnaya, E. Y.; Skorodumova, N. V.; Simak, S. I.; Johansson, B.; Isaev, E. I. Theoretical Study of Linear Monoatomic Nanowires, Dimer and Bulk of Cu, Ag, Au, Ni, Pd and Pt. *Comput. Mater. Sci.* **2008**, *43*, 522–530.
38. Cardarelli, F. *Materials Handbook a Concise Desktop Reference*, 2nd ed.; Springer: London, 2008.